International Journal of Solids and Structures 50 (2013) 1120–1129

Contents lists available at SciVerse ScienceDirect

International Journal of Solids and Structures

journal homepage: www.elsevier.com/locate/ijsolstr

Cyclic plasticity and shakedown in high-capacity electrodes of lithium-ion batteries

Laurence Brassart, Kejie Zhao, Zhigang Suo *

School of Engineering and Applied Sciences and Kavli Institute, Harvard University, Cambridge, MA 02138, United States

ARTICLE INFO

Article history:
Received 19 April 2012
Received in revised form 7 December 2012
Available online 4 January 2013

Keywords:
Diffusion-induced stress
Finite strains
Silicon
Lithium electrodes
Elastic shakedown
Finite element

ABSTRACT

Of all materials, silicon has the highest capacity to store lithium, and is being developed as an electrode for lithium-ion batteries. Upon absorbing a large amount of lithium, the electrode swells greatly, with a volumetric change up to 300%. The swelling is inevitably constrained in practice, often leading to stress and fracture. Evidence has accumulated that the swelling-induced stress can be partially relieved by plastic flow, and that electrodes of small feature sizes can survive many cycles of lithiation and delithiation without fracture. Here we simulate a particle of an electrode subject to cyclic lithiation and delithiation. A recently developed theory of concurrent large swelling and finite-strain plasticity is used to co-evolve fields of stress, deformation, concentration of lithium, and chemical potential of lithium. We identify three types of behavior. When the yield strength is high and the charging rate is low, the entire particle deforms elastically in all cycles. When the yield strength is low and the charging rate is high, the particle (or part of it) undergoes cyclic plasticity. Under intermediate conditions, the particle exhibits the shakedown behavior: part of the particle flows plastically in a certain number of initial cycles, and then the entire particle remains elastic in subsequent cycles. We discuss the effect of the three types of behavior on the capacity and the electrochemical efficiency.

1. Introduction

Rechargeable lithium-ion batteries are energy-storage systems of choice for applications ranging from portable electronics to electric vehicles. Such batteries operate by cyclically inserting lithium into, and extracting lithium from, solid electrodes. As lithium atoms diffuse in and out the electrodes, a field of stress develops and may lead to mechanical degradation of the electrodes. The stress also affects the diffusion process and the electrochemistry of the batteries. Intense research is devoted to developing advanced batteries with improved capacity and reliability (Kasavajjula et al., 2007; Armand and Tarascon, 2008; Whittingham, 2008; Scrosati and Garche, 2010).

A promising research direction focuses on the investigation of new anode materials with high specific capacity, such as lithium alloys (Li_xM; M = Si, Ge, Sn, Al) (Zhang, 2011). Silicon is particularly attractive, as it has the highest theoretical capacity of all materials – each silicon atom can host up to 4.4 atoms of lithium. By contrast, in commercial graphite anodes, every 6 carbon atoms contain up to 1 lithium atom. However, the lithiation of silicon is accompanied by large swelling—a volumetric change up to 300% (Beaulieu et al, 2001). A swelling electrode would be stress-free if each material element in the electrode were unconstrained. In reality, however, the material is inevitably constrained, so that the swelling generates stress, which can cause fracture after a few cycles of charge and discharge (Kasavajjula et al., 2007). Maintaining the mechanical integrity over many cycles of charge and discharge is a bottleneck in developing silicon for commercial high-capacity lithium-ion batteries.

Evidence has accumulated that the lithiation of silicon is accompanied by plastic flow. For instance, thin films of silicon do not recover their initial shape after cyclic lithiation, and undulations develop on the surface of the film (Takamura et al., 2004). In situ measurements in thin films also showed that the stress reaches a yield strength in compression and tension during successive charges and discharges (Sethuraman et al., 2010a,c). The mechanisms of plasticity in lithiated silicon were recently investigated by (Zhao et al., 2011c) using ab initio calculation. Plasticity plays an important role in cycle life of silicon, as it enables large deformation while limiting the stress level. On the other hand, cyclic plasticity is likely to cause mechanical fatigue. While cyclic lithiation is commonly associated with capacity fading in commercial lithium-ion batteries (Ohzuku et al., 1997; Wang et al., 1998), it remains to be clarified how much lithiation-induced plasticity contributes to capacity fading. Plasticity also affects the electrochemical performance of the cell, as mechanical dissipation associated with plastic flow reduces the energy that can be extracted or stored into the material.

The possible role of mechanics on the performance and cycle life of Li-ion batteries has led to intense effort in the modeling of diffusion-induced stresses. A number of continuum theoretical

* Corresponding author. Tel.: +1 617 4953789; fax: +1 617 4960601.
E-mail address: suo@seas.harvard.edu (Z. Suo).

0020-7683/$ - see front matter © 2013 Elsevier Ltd. All rights reserved.
http://dx.doi.org/10.1016/j.ijsolstr.2012.12.019

and numerical studies were conducted on representative microstructures of electrodes, such as spherical particles and nanowires (e.g. Christensen and Newman, 2006a; Zhang et al., 2007; Cheng and Verbrugge, 2009). Most of them rely on the thermal strain analogy and model the lithiation strain as a volumetric, stress-free strain. On the other hand, stress affects the solubility of lithium into the host (Sheldon et al., 2012), an effect which can be accounted for by including an elastic contribution in the expression of the chemical potential (Sethuraman et al., 2010c; Sheldon et al., 2012; Cui et al., 2012), and in that of the diffusivity coefficient (Haftbaradaran et al., 2011).

Recent contributions aimed at extending models to account for the surface reaction kinetics at the electrode/electrolyte interface (Zhang et al., 2007; Golmon et al., 2010; DeLuca et al., 2011), to include the contribution of surfaces stresses (Cheng and Verbrugge, 2008; Deshpande et al., 2010a; Gao and Zhou, 2011) or to account for the variation of material constants with the local concentration of lithium (Deshpande et al., 2010b). Lithiation-induced fracture was also investigated using fracture mechanics (Christensen and Newman, 2006b; Aifantis et al., 2007; Hu et al., 2010; Zhao et al., 2010; Woodford et al., 2010) or cohesive-zone models (Bhandakkar and Gao, 2010, 2011; Grantab and Shenoy, 2012). Most of existing studies assume a linear elastic behavior of the host material and adopt small strain formalism. Models coupling plasticity and diffusion in inelastic electrodes were proposed only very recently (Bower et al., 2011; Zhao et al., 2011a,b; Cui et al., 2012). However, the impact of diffusion-induced plasticity on the cyclic behavior of silicon electrodes is still not well understood.

In this paper we study the mechanical behavior of an elasto-plastic electrode subject to many cycles of lithiation and delithiation. We rely on a recently developed theory of concurrent large swelling and finite-strain plasticity proposed by Zhao et al. (2011a). The theory is written within a consistent thermodynamic framework, and relies on the decomposition of the stretches into elastic, plastic and swelling contribution, the latter being expressed in terms of the local concentration of lithium. We simulate a particle of an electrode subject to many cycles of lithiation and delithiation, and identify three types of behavior: elasticity, cyclic plasticity, and elastic shakedown.

The three types of behavior can be illustrated with a simple example: a thin-film electrode bounded to a rigid substrate (Fig. 1(a)). Lithium is cyclically inserted and extracted at a given rate, and we denote by τ the time needed to reach complete charge or discharge. Let h be the thickness of the film and D be the diffusivity of lithium in the electrode. We consider the limiting case of slow charging, $h << \sqrt{D\tau}$, so that the concentration of lithium is homogeneous within the film. During the insertion of lithium, the film swells in the direction normal to the substrate, while in-plane expansion is constrained, causing in-plane stresses. The stress evolves during the cycle (Fig. 1(b)). Depending on the extent of lithiation, three types of behavior can be identified. When the electrode is cycled between $c = 0$ and $c \leqslant c_1$, the stress remains below the yield strength, and the cyclic deformation is elastic. When the electrode is cycled between $c = 0$ and $c = c_3$, the stress alternately attains the tensile and compressive yield strength and the deformation undergoes cyclic plasticity. When the electrode is cycled between c_2 and c_3, after plasticity in the first cycle, the deformation in the subsequent cycles is elastic, a condition known as shakedown.

For the thin-film electrode, the elastic and shakedown behavior are perhaps of limited practical interest, as they require the electrode to be operated at exceedingly low capacity. This situation is caused by the constraint of the rigid substrate imposed on the electrode. By contrast, in most practical designs of electrodes, small particles of electrode material are embedded in a soft matrix (Wilson et al., 2011; Zhao et al., 2010). The electrode can be considered as free standing, and stresses develop mainly due to the inhomogeneous concentration of lithium. We will show that elastic and shakedown behavior can be encountered in particles for reasonable capacity. We envision that the understanding of these distinct types of behavior will help the design of high-capacity electrodes with enhanced performance and cycle life.

2. Concurrent insertion and plasticity

Consider a free-standing spherical particle of an electrode material (Fig. 2). In the reference state, the particle is stress-free and lithium-free, and the radius of the particle is A. Lithiation and delithiation of the particle is performed by prescribing a nominal flux J_0 of lithium atoms on the surface, corresponding to a given current density operated in a battery cell. At time t, lithium atoms diffuse in the particle, inducing a volumetric change in the electrode. The distribution of the lithium atoms may be inhomogeneous in the radial direction, but is spherically symmetric.

We adopt a recently developed theory of concurrent insertion and finite-strain plasticity (Zhao et al., 2011a). Following a common practice in formulating a field theory, we regard an electrode as a combination of many small material elements, and assume that each element changes in time through a sequence of homogenous states. Communication among the elements is described by

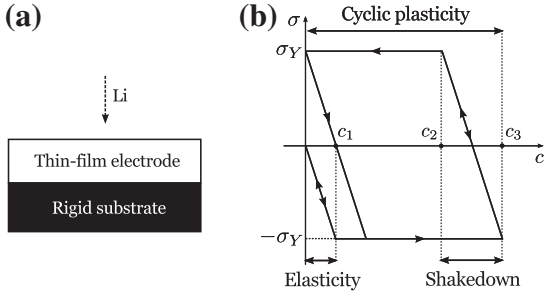

Fig. 1. A thin-film electrode bonded on a rigid substrate is subject to cyclic lithiation and delithiation. During the cycles, the stress in the electrode changes. The electrode is elastic and perfectly plastic, with σ_Y being the yield strength. Depending on the extent of lithiation, the electrode exhibits three types of behavior, marked as elasticity, cyclic plasticity, and shakedown. Cycled between $c = 0$ and $c \leqslant c_1$, the electrode is elastic in all cycles. Cycled between $c = 0$ and $c = c_3$, the electrode undergoes cyclic plasticity. Cycled between c_2 and c_3, the electrode undergoes plastic flow in the first cycle, but is elastic in subsequent cycles, a condition known as shakedown.

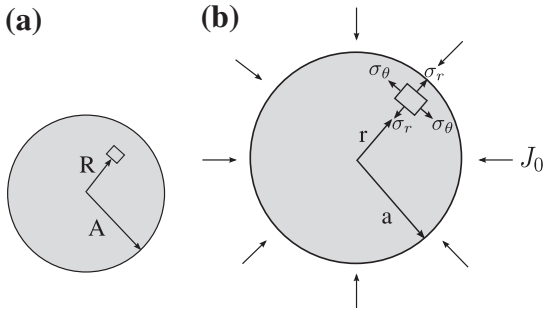

Fig. 2. A spherical particle of an electrode undergoes concurrent insertion reaction and plastic deformation. (a) In the reference state, the particle is lithium-free and stress-free. (b) In the current state, the insertion of lithium causes the particle to swell, and inhomogeneous insertion generates a field of stress within the particle. The charging rate is set by the nominal flux of lithium atoms, J_0.

the kinematics of deformation, balance of forces, conservation of lithium atoms, and kinetics of the migration of lithium atoms.

2.1. Homogeneous states

We first consider the homogeneous states of an individual small element. The theory distinguishes two mechanisms of deformation: elastic and inelastic. Elastic deformation is related to the stretching of bonds between neighboring atoms. Such deformation is recovered when the material element is unloaded. Inelastic deformation involves a rearrangement of atoms and does not necessarily preserves the identity of neighbors. The inelastic stretches are further decomposed into their volumetric and deviatoric parts. It is assumed that the inelastic volumetric change is entirely due to the absorption of lithium—that is, when a unit volume of silicon absorbs C number of lithium atoms, the volume of the lithiated silicon is $1+\Omega C$, where Ω is the volume per lithium atom in silicon. The elastic and inelastic stretches are introduced through a multiplicative decomposition:

$$\lambda_r = \lambda_r^e \lambda_r^p (1+\Omega C)^{1/3}, \quad \lambda_\theta = \lambda_\theta^e \lambda_\theta^p (1+\Omega C)^{1/3}, \tag{1}$$

where λ_r is the stretch, λ_r^e the elastic stretch and λ_r^p the plastic stretch in the radial direction, with λ_θ, λ_θ^e and λ_θ^p being the corresponding stretches in the hoop direction.

We now prescribe the flow rule of plasticity. The plastic stretches are volume preserving:

$$\lambda_r^p (\lambda_\theta^p)^2 = 1. \tag{2}$$

When one plastic stretch is known, (2) gives the other. The material is taken to be elastic and perfectly plastic, with the yield strength σ_Y. Let σ_r be the radial stress and σ_θ be the hoop stress. When $|\sigma_r - \sigma_\theta| < \sigma_Y$, the deformation is elastic, and the plastic stretches remain unchanged. When $|\sigma_r - \sigma_\theta| = \sigma_Y$ but $\delta|\sigma_r - \sigma_\theta| < 0$, the material unloads elastically, and the plastics stretches also remain unchanged. When $|\sigma_r - \sigma_\theta| = \sigma_Y$ and $\delta|\sigma_r - \sigma_\theta| = 0$, the material flows: $\delta \log \lambda_r^p > 0$ if $\sigma_r - \sigma_\theta = \sigma_Y$, and $\delta \log \lambda_r^p < 0$ if $\sigma_r - \sigma_\theta = -\sigma_Y$.

We next specify the equations of state. The radial stress σ_r and the hoop stress σ_θ relate to the elastic stretches by Hooke's law:

$$\begin{aligned} \sigma_r &= \frac{E}{1+\nu}\left[\log \lambda_r^e + \frac{\nu}{1-2\nu}\log\left(\lambda_r^e (\lambda_\theta^e)^2\right)\right], \\ \sigma_\theta &= \frac{E}{1+\nu}\left[\log \lambda_\theta^e + \frac{\nu}{1-2\nu}\log\left(\lambda_r^e (\lambda_\theta^e)^2\right)\right], \end{aligned} \tag{3}$$

where E and ν are Young's modulus and Poisson's ratio, respectively. The chemical potential of lithium in solid solution is assumed to take the following form:

$$\mu = \mu_0 + kT \log\left(\frac{\gamma \Omega C}{\lambda_r \lambda_\theta^2}\right) - \Omega \sigma_m, \tag{4}$$

where $\sigma_m = (\sigma_r + 2\sigma_\theta)/3$ is the mean stress, μ_0 is a reference chemical potential corresponding to that of lithium in the reference electrode, kT is the temperature in the unit of energy, and γ is the activity coefficient. In general, the elastic coefficients E and ν, as well as the yield stress σ_Y are functions of the concentration of lithium (Sethuraman et al., 2010b; Shenoy et al., 2010; Zhao et al., 2011c). However, they are here assumed to be constant for simplicity. A more general expression for the stress-dependent chemical potential (4) would involve the full stress tensor contribution, in addition to the hydrostatic contribution, as recently proposed by Cui et al. (2012). Here, the simpler expression (4) is adopted based on the assumption that the swelling in amorphous silicon is isotropic, so that only the mean stress affects the solubility. Also note that expression (4) was obtained within a consistent thermodynamic framework by Zhao et al. (2011a).

2.2. Inhomogeneous states

We next consider the communication among the material elements. Each material element in the spherical particle is identified by its radius R when the electrode is in the reference state. In the current state at time t, the material element R moves to a position of radius r (Fig. 2). The function $r(R,t)$ fully specifies the kinematics of deformation. The radial and the hoop stretches relate to the function $r(R,t)$ as

$$\lambda_r = \frac{\partial r(R,t)}{\partial R}, \quad \lambda_\theta = \frac{r}{R}. \tag{5}$$

Let $\sigma_r(R,t)$ and $\sigma_\theta(R,t)$ be the radial and hoop stresses. Balance of forces requires that

$$\frac{\partial \sigma_r(R,t)}{\partial R} + \frac{2\lambda_r}{\lambda_\theta R}(\sigma_r - \sigma_\theta) = 0. \tag{6}$$

Let $C(R,t)$ be the nominal concentration of lithium (i.e., the number of lithium atoms per unit volume of pure host in the reference state), and $J(R,t)$ be the nominal flux of lithium (i.e., the number of lithium atoms per unit reference area per unit time). The conservation of the number of lithium atoms requires that

$$\frac{\partial C(R,t)}{\partial t} + \left(\frac{\partial J(R,t)}{\partial R} + \frac{2}{R}J\right) = 0. \tag{7}$$

The flux of lithium in the particle is taken to be proportional to the gradient of the chemical potential:

$$J = -\frac{CD}{kT}\frac{1}{\lambda_r^2}\frac{\partial \mu(R,t)}{\partial R}. \tag{8}$$

The diffusivity D in general depends on the concentration and stresses.

The boundary conditions are prescribed as follows. Spherical symmetry implies that $r(0,t) = 0$ and $J(0,t) = 0$. The surface of the particle is traction free: $\sigma_r(A,t) = 0$, and the nominal flux is prescribed: $J(A,t) = \pm J_0$. The sign differs for charge and discharge. The initial conditions before the first lithiation are $C(R,0) = 0$ and $r(R,0) = R$.

3. Weak formulation

The governing equations presented in the previous section are strongly nonlinear, require a suitable numerical strategy. Here, we implement the model for concurrent insertion and plasticity based on a standard Galerkin finite element formulation within a Lagrangian setting. The coupled equations for stress equilibrium and mass transport are solved simultaneously at every time step, and time-integration is performed using a fully-implicit scheme. The finite element formulation is presented here in a 1D framework, which is sufficient for our purpose. Three dimensional finite element formulation can be found in Zhang et al. (2009) and Bower and Guduru (2012).

The weak formulation for the balance of forces is obtained by a standard procedure. The nominal radial stress P_r and the nominal hoop stress relate to the true stresses as $P_r = \lambda_\theta^2 \sigma_r$ and $P_\theta = \lambda_r \lambda_\theta P_\theta$. In terms of the nominal stresses, the balance of force requires that

$$\frac{\partial P_r(R,t)}{\partial R} + \frac{2}{R}(P_r - P_\theta) = 0. \tag{9}$$

For a given time t, multiplying Eq. (9) by a test function $\hat{u}(R)$ satisfying $\hat{u}(0) = 0$, integrating over the volume of the sphere (accounting for the spherical symmetry) and using integration by parts, we obtain that:

$$\int_0^A \left(P_r \frac{\partial \hat{u}(R)}{\partial R} + 2P_\theta \frac{\hat{u}(R)}{R} \right) R^2 dR = 0. \quad (10)$$

In deriving Eq. (10), we have used the condition that the normal stress on the surface of the particle vanishes. Alternatively, Eq. (10) can be directly obtained from the principle of virtual work.

Similarly, the weak formulation for the conservation of the number of lithium atoms is obtained by first multiplying (7) by another test function $\hat{\mu}(R)$ and integrating over the volume of the particle, which yields:

$$\int_0^A \left(\frac{\partial C(R,t)}{\partial t} + \frac{\partial J(R,t)}{\partial R} + \frac{2}{R} J \right) \hat{\mu} R^2 dR = 0. \quad (11)$$

The flux satisfies the boundary conditions $J(0,t) = 0$ and $J(A,t) = \pm J_0$, where the sign is positive during delithiation, and negative during lithiation. Integrating (11) by parts, we obtain that

$$\int_0^A \left(\frac{\partial C(R,t)}{\partial t} \hat{\mu}(R) - J \frac{\partial \hat{\mu}(R)}{\partial R} \right) R^2 dR \pm J_0 \hat{\mu}(A) A^2 = 0. \quad (12)$$

The weak form (12) suggests the use of the chemical potential $\mu(R,t)$ as primary unknown for the transport problem, instead of the concentration $C(R,t)$.

In Eq. (10), the stresses are related to the displacement and concentration through the elastoplastic constitutive model described in Section 2.1. In Eq. (12), the concentration is computed from the chemical potential and the stress according to the constitutive Eq. (4), while the flux is given by Eq. (8). Hence, Eqs. (10) and (12) are strongly coupled, and are solved simultaneously. In a time-discretized setting, the time derivative of the concentration in Eq. (12) is estimated by (fully-implicit) backward differences. Time integration of the plasticity equations over every time step is performed using a standard, fully-implicit radial return scheme (see e.g. Simo and Hughes, 1998).

At every time step Eqs. (10) and (12) are discretized in space over N elements using linear shape functions to interpolate the unknown fields $u(R,t)$ and $\mu(R,t)$. Integrals are computed numerically using the Gauss method with one integration point at the center of every element. The finite element discretization yields a system of $2N$ nonlinear equations which is solved at every time step using a Newton–Raphson scheme. All numerical results presented in the sequel were obtained using 120 non-uniformly distributed nodes along the radius. The mesh was refined close to the free boundary in order to capture the natural boundary condition on the stress accurately. Convergence of the results was verified against results obtained on refined meshes.

4. Numerical results and discussions

In numerical simulations we take the following values for various parameters. The spherical particle in the stress-free, lithium-free state is of radius $A = 1$ μm. Material parameters of the electrode are representative of amorphous lithiated silicon: $E = 80$ GPa, $\nu = 0.3$, $\sigma_Y = 0.5$ GPa, $D = 10^{-16}$ m^2/s (Ding et al., 2009; Sethuraman et al., 2010a). A representative value for the volume of a lithium atom in silicon is $\Omega = 1.36 \times 10^{-29}$ m^3. The activity coefficient γ in general depends on composition. Experimental measurements of this dependence were not reported so far in the literature, but important deviation from ideality should be expected. As we are mostly concerned with mechanics, here, for simplicity, we set $\gamma = 1$. The temperature is $T = 300$ K. The maximum theoretical concentration of lithium in silicon C_{max} is estimated from the observation that the volume of fully lithiated silicon is about 300%, so that $\Omega C_{max} \approx 3$. The flux J_0 can be related to the theoretical nominal time τ needed to uniformly lithiate the particle to the maximum theoretical concentration as: $4\pi A^2 J_0 \tau = (4\pi A^3/3) C_{max}$, such that $J_0 = AC_{max}/3\tau$. In our simulations, we prescribe the value of the nominal time τ, and keep the maximum theoretical concentration C_{max} constant. Throughout the discussion dimensionless quantities are used. Time is normalized as Dt/A^2, where the diffusion time scale is $A^2/D = 10^4$ s. The boundary value problem is characterized by three dimensionless parameters: $\Omega\sigma_Y/kT$, σ_Y/E and $J_0 A\Omega/D = A^2/\tau D$. The first one characterizes the ratio between stress and chemical contribution in the expression (4) of the chemical potential. The second one gives the order of magnitude of the elastic strains. The third one represents the dimensionless charging rate.

We first consider the initial lithiation of the particle at rate $\tau = 1$ h, which corresponds to a normalized injection rate $J_0 A\Omega/D = 2.8$. The simulation is initiated when the particle is lithium-free and stress-free, and terminated when the concentration reaches the maximum theoretical capacity C_{max} on the surface. Various fields are plotted at several times during lithiation (Fig. 3). Both the concentration and the chemical potential of lithium are inhomogeneous. The gradient of the chemical potential drives lithium atoms to diffuse towards the center of the particle, but the gradient decreases with time. When concentration on the surface of the particle reaches C_{max}, the concentration at the center of the particle is still a fraction of C_{max} —that is, at this injection rate, the particle is unable to be fully lithiated. Because of the inhomogeneous concentration, the particle swells more on the surface than at the center.

The inhomogeneous swelling is accommodated by elastic and plastic deformation, which in turn generates a field of stress. The radial stress σ_r is tensile in the particle and vanishes on the surface. The hoop stress σ_θ is tensile near the center, and compressive near the surface. The mean stress has a similar trend (Fig. 3(c)). According to (4), a tensile mean stress reduces the chemical potential of lithium, and a compressive mean stress increases the chemical potential of lithium. Consequently, the gradient of mean stress tends to promote lithium to diffuse toward the center. The evolution of the mean stress with time is non-monotonic: the tensile mean stress near the center first increases with time, before decreasing. However, it is always maximum at the center, and may exceed the value of the yield stress. The equivalent stress is given by $\sigma_e = |\sigma_\theta - \sigma_r|$. For a perfectly plastic material, $\sigma_e < \sigma_Y$ when material deforms elastically, and $\sigma_e = \sigma_Y$ when the material yields. At the center of the particle, $\sigma_\theta = \sigma_r$ and $\sigma_e = 0$. Plasticity develops in the outer region of the particle. In the early stages of lithiation, the plastic region progresses towards the center of the article, as seen from the curves for $Dt/A^2 = 0.01$ and 0.025 (Fig. 3(d)). Then, due to the progressive homogenization of concentration in the plastic region, the equivalent stress decreases and the material unloads elastically (Fig. 4).

The fields are affected by the injection rate (Fig. 5). Shown here are fields at the end of lithiation, when the concentration reaches C_{max} on the surface of the particle. When the injection rate decreases (or, equivalently, the charging time τ increases), the concentration profiles becomes more homogeneous. For the slowest injection rate considered here ($\tau = 4$ h), the concentration at the center is above 90% of the maximum concentration. By contrast, when the injection rate is very fast ($\tau = 0.25$ h), the concentration of lithium is close to zero in a large inner core of the particle. Lithium atoms then accumulate in a narrow shell of the particle, as they do not have the time to diffuse inwards. The gradient of chemical potential is also found to increase as the charging rate increases. The strongly inhomogeneous concentration observed at high charging rate is accompanied by high stress levels. For $\tau = 0.25$ and $\tau = 0.5$ h, some outer shell of the particle deforms plastically during the entire lithiation process. By contrast, all other injection rates considered here enable elastic unloading. Also, the extent of the plastic region is smaller for $\tau = 0.25$ h than for $\tau = 0.5$ h. Indeed, for $\tau = 0.25$ h the concentration in lithium and

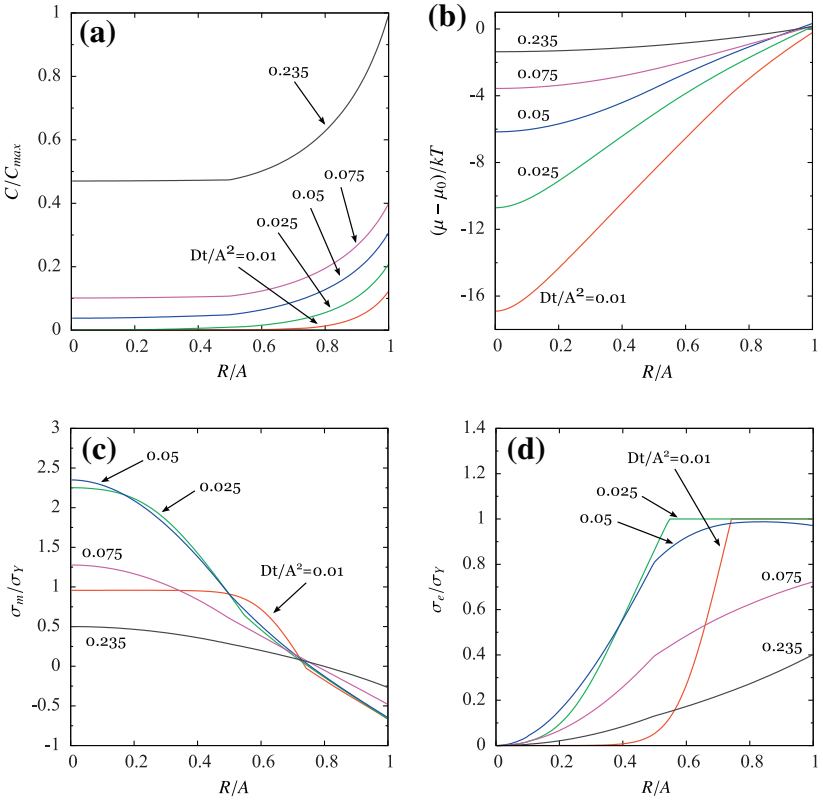

Fig. 3. Fields in an electrode at several times during initial lithiation at rate $\tau = 1$ h: (a) concentration of lithium, (b) chemical potential of lithium, (c) mean stress, and (d) equivalent stress.

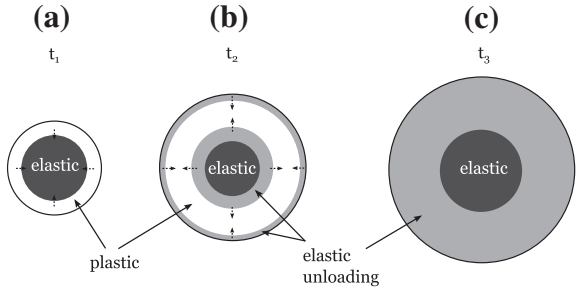

Fig. 4. At a moderate charging rate, some material elements undergo plastic flow followed by elastic unloading. (a) During early stages of lithiation, the outer shell of the particle plastically flows, while the inner core remains elastic. The plastic flow results from the high compressive stress due to the inhomogeneous distribution of lithium. As lithium diffuses towards the center of the particle, the plastic zone also progresses towards the center. (b) The progressive homogenization of lithium reduces the stress, and the material elements unload elastically, starting on the outer surface of the particle and in the vicinity of the elastic core. (c) Eventually, the entire outer shell unloads elastically.

its accompanying volume expansion are virtually zero in a significant inner region of the particle. The stress state is mostly hydrostatic and tensile, and equilibrates the compressive stress of the outer shell. For $\tau = 0.5$ h, some lithium has time to reach inner regions of the particle, and plasticity develops in a larger region of the particle.

These results show that the particle may unload elastically after initial plastic yielding for a moderate injection rate. For very slow rate, the deformation mode may even remain elastic during the entire process of lithium insertion. We may thus distinguish three types of behavior for the initial lithiation: elastic, plastic and plastic followed by elastic unloading. The different types of behavior are identified from the value of the hoop stress on the surface of the particle. Obviously, the operating mode of the particle depends on material parameters, in addition to the injection rate. We identify the three types on a plane spanned by $A^2/\tau D$ (the dimensionless injection rate) and $\Omega\sigma_Y/kT$ (the normalized yield strength) (Fig. 6). Here the yield strength is normalized by $kT/\Omega = 304$ MPa. If the particle is lithiated at low injection rate and if the yield strength is high, the particle deforms purely elastically. On the other hand, for a fast injection rate and sufficiently low yield stress, some outer shell of the particle deforms plastically during the whole lithiation process. Other combinations of yield stress and charging rates lead to plastic flow followed by elastic unloading.

We next consider the first delithiation at rate $\tau = 1$ h (Fig. 7). The initial conditions are given by the fields obtained for the last time step of the first lithiation. Hence, the profiles for $Dt/A^2 = 0$ in Fig. 7 coincide with those for $Dt/A^2 = 0.235$ in Fig. 3. The simulation is ended when the surface concentration of lithium reaches 1%. At the end of the simulation, the concentration at the center of the particle is about 5%. Lithium is driven out of the particle by the gradient in the chemical potential. The latter tends to $-\infty$ on the surface as the concentration of lithium tends to zero. As lithium is extracted, the outer part of the particle contracts more than the inner part. Consequently, the hoop stress is tensile on the surface, and the center in under hydrostatic compression. The gradient of mean stress contributes to the diffusion of lithium towards the surface. Profiles of the equivalent stress indicate that the deformation is elastic for $Dt/A^2 \leqslant 0.12$, and subsequently plastic. Plasticity causes the abrupt change in the slope of the concentration profiles for $Dt/A^2 = 0.18$ and $Dt/A^2 = 0.21$.

We now simulate consecutive cycles of lithiation and delithiation of the particle. The sign of the nominal injection flux is changed when the surface concentration of lithium reaches 100%

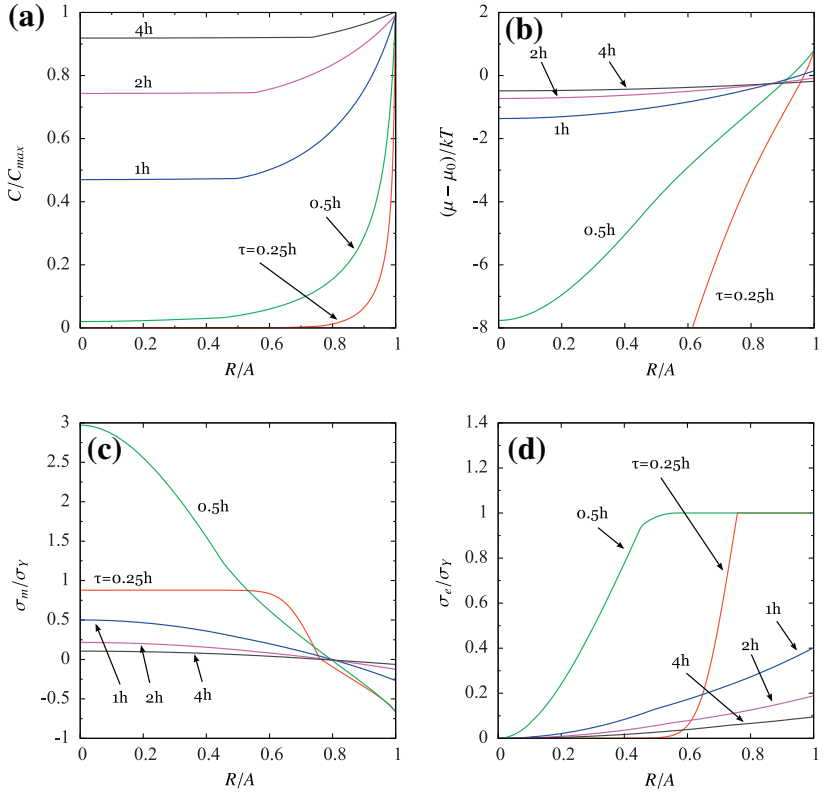

Fig. 5. Fields attained at the end of initial lithiation at several charging rates: (a) concentration of lithium, (b) chemical potential of lithium, (c) mean stress, and (d) equivalent stress.

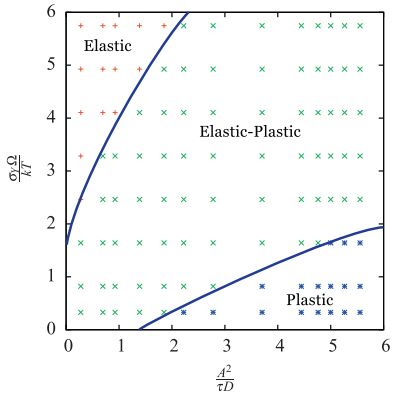

Fig. 6. During initial lithiation, the electrode can exhibit three types of behavior, as identified by different regions on the plane spanned by the yield strength and the rate of lithiation. When the yield strength is high and the charging rate is low, the entire particle remains elastic at all time. When the yield strength is low and the charging rate is high, the outer surface flows plastically during the whole lithiation process. The intermediate region corresponds to the behavior that some region of the particle flows plastically, followed by elastic unloading. Each point in the plane corresponds to one simulation with given values of the yield strength and the charging rate. Also marked are the approximate boundaries between the regions of different types of behavior.

(lithiation) or 1% (delithiation). We investigate the conditions under which plasticity develops within the particle, as well as the impact of plasticity on the capacity of the electrode. Since plastic flow always initiates from the surface, according to our preliminary results for the initial lithiation, we use the value of the hoop stress on the surface to detect plastic flow. The total amount of lithium absorbed during lithiation divided by the maximum theoretical capacity defines the *normalized lithiation capacity*:

$$\overline{C} = \frac{\int C(R,t_f)dV - \int C(R,t_i)dV}{4\pi A^3 C_{\max}/3}, \tag{13}$$

where t_i and t_f are the time at the beginning and the end of the lithiation, respectively. A delithiation capacity can be similarly defined computing the amount of lithium extracted. The ratio of the delithiation capacity and the lithiation capacity defines the *efficiency*. The capacity and efficiency introduced here should be understood as theoretical quantities under constant current loading conditions only. Furthermore, the present analysis does not account for other physico-chemical mechanisms which are known to affect capacity and efficiency, such as the formation of solid-electrolyte interface (SEI) or fracture.

Fig. 8 shows the evolution of the surface hoop stress, lithiation capacity and efficiency after several cycles of lithiation and delithiation. Three nominal lithiation rates are considered: $\tau = 0.5$ h (Fig. 8(a) and (b)), $\tau = 1$ h (Fig. 8(c) and (d)) and $\tau = 10$ h (Fig. 8(e) and (f)). The evolution of the hoop stress on the surface is presented only for the first five cycles. Each one of the considered lithiation rates leads to a distinct type of behavior. For the fastest lithiation rate ($\tau = 0.5$ h), the surface of the particle constantly undergoes plastic flow, except during the elastic unloading parts of the curve corresponding to the sign change in the injection flux. The stress evolution on the surface looks then very similar to biaxial stress in the thin film (Fig. 1). This situation corresponds to a poor capacity (Fig. 8(b)). Note also that eight cycles are needed to reach a steady-state behavior, as apparent from the efficiency curve. For $\tau = 1$ h, the evolution of the surface stress shows plastic yielding in compression followed by elastic unloading during lithiation, and elastic deformation followed by plastic yielding in tension during delithiation (Fig. 8(c)), consistently with previous results presented in Figs. 3 and 7. In this case the steady-state behavior is reached after only four cycles, and the capacity is close

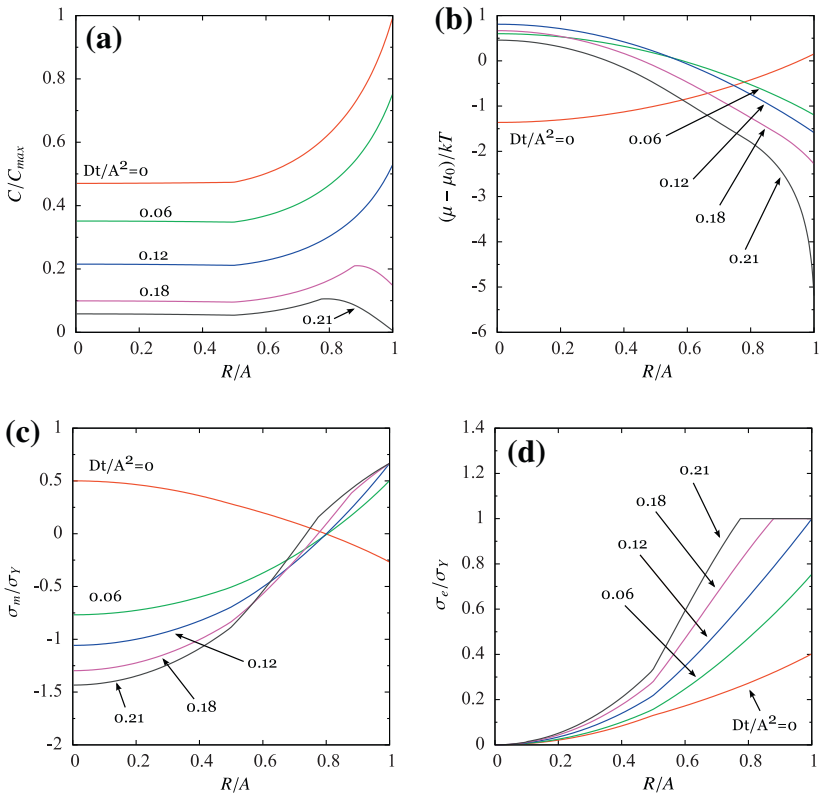

Fig. 7. Fields in a particle at several times during delithiation: (a) concentration of lithium, (b) chemical potential of lithium, (c) mean stress, and (d) equivalent stress. The rate of delithiation is the same as the rate of lithiation in Fig. 3. The initial conditions at $Dt/A^2 = 0$ coincide with the fields in the particle at the end of the initial lithiation (i.e., the profiles for $Dt/A^2 = 0.235$ in Fig. 3.

to 80%. For $\tau = 10$ h, plastic flow briefly takes place during the first cycle, both during lithiation (in compression) and delithiation (in tension) (Fig. 8(e)). However, all subsequent cycles remain entirely elastic: the absolute value of the surface hoop stress remains lower than the yield stress. In this case the capacity is almost 100% from the second cycle (Fig. 8(f)).

Results for $\tau = 0.5$ h illustrate the purely plastic operating mode and represent the cyclic counterpart to the plastic regime represented in the map of Fig. 6. Similarly, results for $\tau = 1$ h illustrate the situation of plastic deformation followed by elastic unloading under cyclic load. The operating mode obtained taking $\tau = 10$ h could not be represented in the map of Fig. 6, as it can be defined only for cyclic loading. This mode is achieved when lithiation/delithiation cycles first lead to plastic flow on the surface during the transition to the regime situation, while the latter is entirely elastic. We refer to this mode as "elastic shakedown", and similar to that in the thin-film electrode (Fig. 1). Finally, the fully elastic regime can be reached considering even slower injection rates. This case is not represented in Fig. 8.

The numerical results indicate that the number of cycles needed to reach steady-state increases with the injection rate. This behavior can be qualitatively understood as follows. In the initial configuration, the particle is concentration-free and stress-free. After the first lithiation/delithiation cycle, due to the diffusion kinetics, there remains a certain amount of lithium within the particle, as illustrated in Fig. 7(a). The permanent plastic deformations that were generated during the first cycle also induce residual stresses, see Fig. 7(c) and (d). Therefore, the state of the particle at the beginning of the second lithiation/delithiation cycle is different from the initial state, and the concentration and stress fields which will develop during the second cycle will also differ from those which developed during the first cycle. The same reasoning can be applied cycle after cycle, leading to the transient behavior observed in Fig. 8(b) and (d), and, to a lesser extent, in Fig. 8(e).

Fig. 9 shows a map of the different regimes which can be encountered during lithiation/delithiation cycles. The map was constructed considering many combinations of charging rates (between $\tau = 0.5$ h and $\tau = 10$ h) and yield stresses (between $\sigma_Y = 0.1$ GPa and $\sigma_Y = 2$ GPa). Other material parameters were kept constant. Every point in the map represents one simulation of 10 cycles, ensuring that regime is reached. The operating regimes (elastic, elastic shakedown and plastic) were determined from the value of the surface hoop stress. The map also represents some iso-value lines for the normalized capacity $\overline{C}$ computed after the 10^{th} charge and discharge according to Eq. (13). Obviously, the elastic and elastic shakedown modes enable excellent capacity of the electrode in regime. A very good capacity may also be obtained when cycles are partially elastic and partially plastic. The purely plastic mode is associated with poor capacity, and corresponding points are all located below the 50% iso-line in the figure. Note that the effect of varying Young's modulus is not represented on the map. The impact of the elastic stiffness on the deformation regimes is not very significant, as the stress is limited by the yield stress. A notable exception is the center of particle, which is always under hydrostatic tension or compression. The stress at the center of the particles then scales with Young's modulus.

The operating regime is expected to affect the mechanical degradation of the electrode in service. The cyclic plasticity regime (as encountered in Fig. 8(a) and (b)) is the most likely to lead to damage after many cycles due to fatigue, due to the repeated plastic straining in opposite directions during each part of the cycle. The absolute value of surface hoop stress is then also equal to its upper bound (the yield strength) during the major portion of the cycle. Conversely, elastic or elastic shakedown modes are more

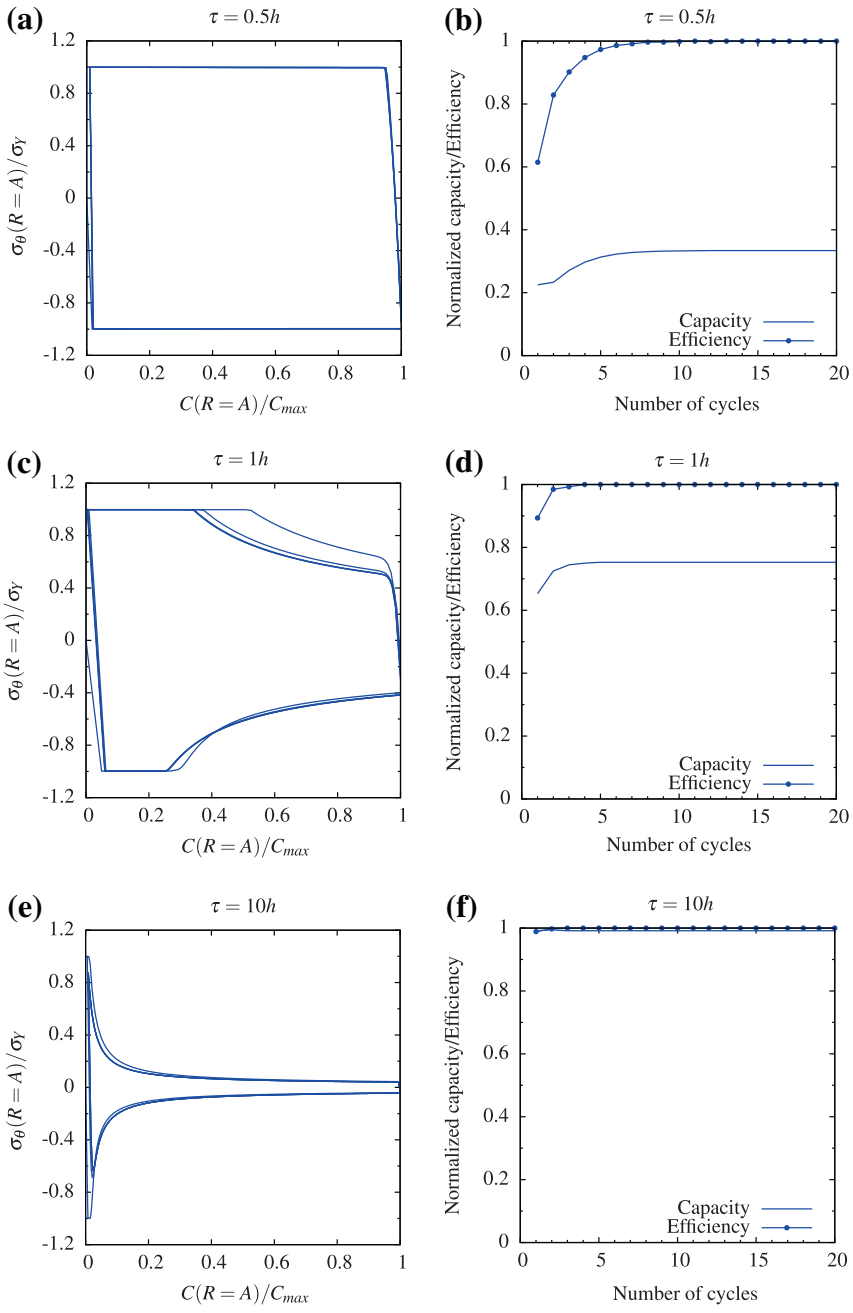

Fig. 8. Responses of a spherical particle during consecutive cycles of lithiation and delithiation. (a), (c) and (e) show five cycles on the plane spanned by the hoop stress at the surface and the concentration at the surface. (b), (d) and (f) show the normalized capacity and efficiency as a function of the number of cycles. Depending on the charging rate, distinct dominant deformation mechanisms are identified: (a) and (b) cyclic plasticity (τ = 0.5 h), (c) and (d) plasticity followed by elastic unloading (τ = 1 h) and shakedown (τ = 10 h).

favorable to avoid fatigue. It is therefore highly desirable to be able to predict when plastic cycling occurs, based on the material properties of the host, the lithiation/delithiation rate and the geometry of the host (the effect of the latter was not specifically studied in the present work). For this purpose, maps such as presented in Fig. 9 are valuable tools.

Note that the existence of distinct operating regimes in engineering problems involving plastic deformations and transport problem is not new. For instance, Bree (1967) considered elastoplastic thin tubes subject to a constant internal pressure and cyclic thermal loading. In that case, four operating regimes could be distinguished, namely elasticity, cyclic plasticity, elastic shakedown and ratcheting, and were reported within maps similar to Fig. 9. In that problem, thermal equilibrium was assumed. In contrast, the different types of behavior reported here directly follow from the non-equilibrium response in the transport problem. Indeed, they result from the competition between lithium insertion and extraction on the boundary of the particle at a given rate, and the diffusion of lithium throughout the host. Also note that ratcheting was not observed in the present case. Ratcheting was recently reported by Haftbaradaran and Gao (2012) in the case of thin films, as a consequence of an assumed asymmetry in the behavior of the host in tension and compression, which was not considered here.

The value of the chemical potential on the surface of the electrode can be used to estimate the open circuit potential of the electrode as:

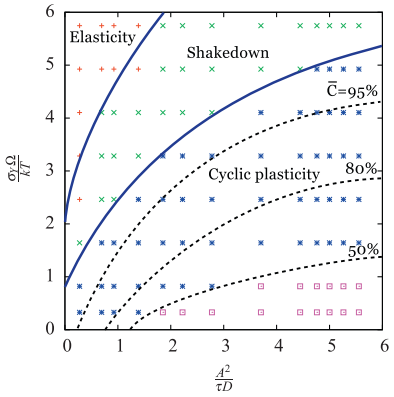

Fig. 9. Marked on the plane spanned by the yield strength and the injection rate are three types of cyclic behavior: elasticity, shakedown, and cyclic plasticity. The regimes are identified from the value of the surface hoop stress. In the elastic regime, the volume expansion is accommodated by elastic strains only. In the cyclic plasticity regime, the surface undergoes plastic yielding during part of the lithiation/delithiation process. The shakedown regime is achieved when the regime cycle is entirely elastic, although plasticity develops during initial cycles. In the figure, each point corresponds to one simulation with given values of yield strength and rate of lithiation and delithiation. The blue lines highlight the (approximate) boundaries between different regimes. The dashed lines represent (approximate) iso-values of the normalized lithiation capacity. All points located below the 50% iso-value line correspond to a cyclic plasticity regime without elastic unloading (except during load reversal).

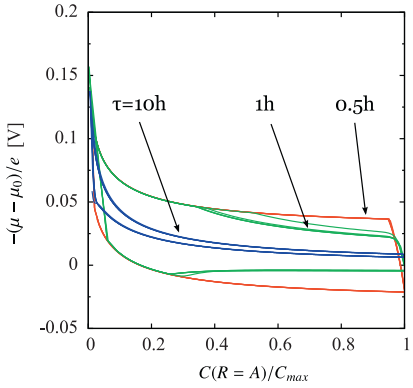

Fig. 10. Plasticity-induced hysteresis of the open circuit voltage as a function of the surface concentration of lithium. Results are shown here for the first 5 cycles. Hysteresis is more pronounced for lithiation with a fast charging rate, as the deformation mode is dominated by plasticity. Hysteresis can be significantly reduced when the electrode is operated under the conditions of shakedown and elasticity.

$$\Phi = -\frac{\mu - \mu_0}{e}, \tag{14}$$

where e is the elementary charge: $e = 1.602 \times 10^{-19}$ C. Expression (14) is obtained from the balance of the free energy change due to chemical reaction and electric energy. Therefore, the voltage (14) must be understood as the instantaneous *open circuit* potential that would be observed between the silicon electrode and a reference electrode of lithium metal with potential μ_0. The voltage (14) accounts for the stress on the surface of the particle, according to expression (4) of the chemical potential. A tensile stress promotes lithiation and, consequently, increases the open cell voltage. Conversely, a compressive state of stress on the surface raises the chemical potential and decreases the open cell voltage. Following Sethuraman et al. (2010c), the intensity of the stress-potential coupling at a given state of charge can be quantified by:

$$\frac{\partial \Phi}{\partial \sigma_m} = \frac{\Omega}{e} = 85 \text{ mV/GPa}. \tag{15}$$

Here, Eqs. (14) and (15) are used at the surface of the electrode, were the voltage is computed. These expression are however very general, as they only use local values of stress and composition. In particular, they do not depend on the particular geometry of the electrode.

Fig. 10 shows the evolution of the open circuit potential of the electrode during the 5 first cycles of lithiation/delithiation. The electrode potential demonstrates pronounced hysteresis, which follows from the corresponding hysteresis in the stress response during lithiation and delithiation. Its magnitude is directly linked to the intensity of the stress-potential coupling (15). The latter can be retrieved from the numerical results in Figs. 9 and 10 taking the ratio of the slopes of the voltage–concentration curve and the corresponding stress-concentration curves. For instance, for the case $\tau = 0.5$ h in Figs. 9(a) and 10, the potential change computed during the elastic part of the cycle during which the surface hoop stress goes from $-\sigma_Y$ to σ_Y (i.e., $\Delta\sigma_m = 4\sigma_Y/3 = 0.67$ GPa) is about 60 mV, as expected from (15). A similar value of the stress-potential coupling was experimentally observed by Sethuraman et al. (2010c) in the case of thin film electrodes. The magnitude of the stress effect on the open cell potential is also consistent with the value computed by Sheldon et al. (2012).

Hysteresis is here the direct consequence of the dissipated mechanical energy during plastic flow. Accordingly, hysteresis is more pronounced for fast injection rates, which correspond to the cyclic plasticity operating regime. Note that significant hysteresis in the cell voltage response is observed in the elastic shakedown case (for $\tau = 10$ h in the figure), although deformations remain elastic in regime. The voltage hysteresis is linked to the offset in the stress response in tension and compression for concentration resulting from the permanent plastic strains which developed during initial cycles.

The voltage–concentration curve presented in Fig. 10 qualitatively reproduces typical experimental voltage–concentration curve, see e.g. (Sethuraman et al. (2010a)). In that paper, the measured voltage of a cell consisting of an amorphous silicon thin film and a lithium metal reference electrode ranged from about 0.05 to 1.2 V when charged at rate C/4. By comparison, the voltage computed here is significantly lower, which can be explained by the fact that it actually corresponds to the open-cell voltage of a pre-stressed electrode. Therefore, it does not account for sources of dissipation other than plasticity, as chemical reactions at the electrolyte/electrode interface, and other internal resistances. Moreover, the thin film configuration significantly differs from the spherical configuration, as the thin film experiences the constraint of the substrate even under very low injection rate. Finally, expression (4) for the chemical potential was used under the assumption of ideal solution, which is most probably not accurate when the concentration of lithium is high.

5. Conclusions

We have simulated lithiation/delithiation cycles of a spherical electrode at given injection rates using a continuum theory of concurrent diffusion and finite-strain plasticity. Three types of behavior are identified: elastic, plastic and elastic shakedown. Which behavior operates depends on the injection rate and the material parameters. Here, we reported maps of the operating modes obtained under various combinations of the yield stress of the host and the injection rate. In particular, elastic and elastic shakedown modes are obtained when the charging rate is slow and the yield stress is high. These modes correspond to low surface stress, and enable excellent capacity and efficiency of the electrode after a few cycles. The hysteresis in the voltage vs. capacity plot is also significantly reduced. By contrast, a fully plastic operating mode

is associated with low capacity, high stress levels and significant mechanical energy losses.

Acknowledgements

This work is supported by the National Science Foundation through a Grant on Lithium-ion Batteries (CMMI-1031161). L. B. acknowledges the support of the Belgian American Educational Foundation (BAEF) and that of the Special Fund for Research of Belgium (FSR) through a FSR-UCL grant.

References

Aifantis, K.E., Hackney, S.A., Dempsey, J.P., 2007. Design criteria for nanostructured Li-ion batteries. Journal of Power Sources 165, 874–879.

Armand, M., Tarascon, J.-M., 2008. Building better batteries. Nature 451, 652–657.

Beaulieu, L.Y., Eberman, K.W., Turner, R.L., Krause, L.J., Dahn, J.R., 2001. Colossal reversible volume changes in lithium alloys. Electrochemical and Solid-State Letters 4, A137–A140.

Bhandakkar, T.K., Gao, H., 2010. Cohesive modeling of crack nucleation under diffusion induced stresses in a thin strip: implications on the critical size for flaw tolerant battery electrodes. International Journal of Solids and Structures 47, 1424–1434.

Bhandakkar, T.K., Gao, H., 2011. Cohesive modeling of crack nucleation in a cylindrical electrode under axisymmetric diffusion induced stresses. International Journal of Solids and Structures 48, 2304–2309.

Bower, A.F., Guduru, P.R., 2012. A simple finite element model of diffusion, finite deformation, plasticity and fracture in lithium ion insertion electrode materials. Modelling and Simulation in Material Science and Engineering 20, 045004.

Bower, A.F., Guduru, P.R., Sethuraman, V.A., 2011. A finite strain model of stress, diffusion, plastic flow, and electrochemical reactions in lithium-ion half-cell. Journal of the Mechanics and Physics of Solids 59, 804–828.

Bree, J., 1967. Elastic–plastic behaviour of thin tubes subjected to internal pressure and intermittent high-heat fluxes with application to fast-nuclear-reactor fuel elements. Journal of Strain Analysis 2, 226–238.

Cheng, Y.-T., Verbrugge, M.W., 2008. The influence of surface mechanics on diffusion induced stresses within spherical nanoparticles. Journal of Applied Physics 104, 083521.

Cheng, Y.-T., Verbrugge, M.W., 2009. Evolution of stress within a spherical insertion electrode particle under potentiostatic and galvanostatic operation. Journal of Power Sources 190, 453–460.

Christensen, J., Newman, J., 2006a. Stress generation and fracture in lithium insertion materials. Journal of Solid State Electrochemistry 10, 293–319.

Christensen, J., Newman, J., 2006b. A mathematical model of stress generation and fracture in lithium manganese oxide. Journal of the Electrochemical Society 153, A1019–A1030.

Cui, Z., Gao, F., Qu, J., 2012. A finite deformation stress-dependent chemical potential and its application to lithium ion batteries. Journal of the Mechanics and Physics of Solids 60, 1280–1295.

DeLuca, C.M., Maute, K., Dunn, M.L., 2011. Effects of electrode particle morphology on stress generation in silicon during lithium insertion. Journal of Power Sources 196, 9672–9681.

Deshpande, R., Cheng, Y.-T., Verbrugge, M.W., 2010a. Modeling diffusion-induced stress in nanowire electrode structure. Journal of Power Sources 195, 5081–5088.

Deshpande, R., Qi, Y., Cheng, Y.-T., 2010b. Modeling of concentration-dependent elastic modulus on diffusion-induced stresses for battery applications. Journal of the Electrochemical Society 157, A967–A971.

Ding, N., Xu, J., Yao, Y.X., Wegner, G., Fang, X., Chen, C.H., Lieberwirth, I., 2009. Determination of the diffusion coefficient of lithium ions in nano-Si. Solid State Ionics 180, 222–225.

Gao, Y.F., Zhou, M., 2011. Strong stress-enhanced diffusion in amorphous lithium alloy nanowire electrodes. Journal of Applied Physics 109, 014310.

Golmon, S., Maute, K., Lee, S.-H., Dunn, M.L., 2010. Stress generation in silicon particles during lithium insertion. Applied Physics Letters 97, 033111.

Grantab, R., Shenoy, V.B., 2012. Pressure-gradient dependent diffusion and crack propagation in lithiated silicon nanowires. Journal of the Electrochemical Society 159, A584–A591.

Haftbaradaran, H., Gao, H., 2012. Ratcheting of silicon island electrodes on substrate due to cyclic intercalation. Applied Physics Letters 100, 121907.

Haftbaradaran, H., Song, J., Curtin, W.A., Gao, H., 2011. Continuum and atomistic models of strongly coupled diffusion, stress, and solute concentration. Journal of Power Sources 196, 361–370.

Hu, Y.H., Zhao, X.H., Suo, Z.G., 2010. Averting cracks caused by insertion reaction in lithium-ion batteries. Journal of Materials Research 25, 1007–1010.

Kasavajjula, U., Wang, C., Appleby, A.J., 2007. Nano- and bulk-silicon based insertion anodes for lithium-ion secondary cells. Journal of Power Sources 163, 1003–1039.

Ohzuku, T., Tomura, H., Sawai, K., 1997. Monitoring of particle fracture by acoustic emission during charge and discharge of $LiMnO_2$ cells. Journal of the Electrochemical Society 144, 3450–3496.

Scrosati, B., Garche, J., 2010. Lithium batteries: status, prospects and future. Journal of Power Sources 195, 2419–2430.

Sethuraman, V.A., Chon, M.J., Shimshak, M., Srinivasan, V., Guduru, P.R., 2010a. In situ measurements of stress evolution in silicon thin films during electrochemical lithiation and delithiation. Journal of Power Sources 195, 5062–5066.

Sethuraman, V.A., Chon, M.J., Shimshak, M., Van Winckle, N., Guduru, P.R., 2010b. In situ measurements of biaxial modulus of Si anodes for Li-ion batteries. Electrochemistry Communications 12, 1614–1617.

Sethuraman, V.A., Srinivasan, V., Bower, A.F., Guduru, P.R., 2010c. In situ measurements of stress-potential coupling in lithiated silicon. Journal of the Electrochemical Society 157, A1253–A1261.

Sheldon, B.W., Soni, S.K., Xiao, X., Qi, Y., 2012. Stress contributions to solution thermodynamics in Li–Si alloys. Electrochemical and Solid-State Letters 15, A9–A11.

Shenoy, V.B., Johari, P., Qi, Y., 2010. Elastic softening of amorphous and crystalline Li–Si phases with increasing Li concentration: a first-principles study. Journal of Power Sources 195, 6825–6830.

Simo, J.C., Hughes, T.J.R., 1998. Computational Inelasticity. Springer.

Takamura, T., Ohara, S., Uehara, M., Suzuki, J., Sekine, K., 2004. A vacuum deposited Si film having a Li extraction capacity over 2000 m Ah/g with a long cycle life. Journal of Power Sources 129, 96–100.

Wang, H., Jang, Y., Huang, B., Sadoway, D.R., Chiang, Y., 1998. TEM study of electrochemical cycling-induced damage and disorder in $LiCoO_2$ cathodes for rechargeable lithium batteries. Journal of the Electrochemical Society 146, 473–480.

Whittingham, M.S., 2008. Materials challenges facing electrical energy storage. MRS Bulletin 33, 411–419.

Wilson, J.R., Cronin, J.S., Barnett, S.A., Harris, S.J., 2011. Measurement of three-dimensional microstructure in a $LiCoO_2$ positive electrode. Journal of Power Sources 196, 3443–3447.

Woodford, W.H., Chiang, Y.-M., Carter, W.C., 2010. "Electrochemical shock" of intercalation electrodes: a fracture mechanics analysis. Journal of the Electrochemical Society 157, A1052–A1059.

Zhang, W.J., 2011. A review of the electrochemical performance of alloy anodes for lithium-ion batteries. Journal of Power Sources 196, 13–24.

Zhang, X., Sastry, A.M., Shyy, W., 2007. Numerical simulation of intercalation-induced stress in Li-ion battery electrode particles. Journal of the Electrochemical Society 154, A910–A916.

Zhang, J.P., Zhao, X.H., Suo, Z.G., Jiang, H.Q., 2009. A finite element method for transient analysis of concurrent large deformation and mass transport in gels. Journal of Applied Physics 105, 093522.

Zhao, K.J., Pharr, M., Vlassak, J.J., Suo, Z.G., 2010. Fracture of electrodes in lithium-ion batteries caused by fast charging. Journal of Applied Physics 108, 073517.

Zhao, K.J., Pharr, M., Cai, S., Vlassak, J.J., Suo, Z.G., 2011a. Large plastic deformation in high-capacity lithium-ion batteries caused by charge and discharge. Journal of the American Ceramic Society 94, S226–S235.

Zhao, K.J., Pharr, M., Vlassak, J.J., Suo, Z.G., 2011b. Inelastic hosts as electrodes for high capacity lithium-ion batteries. Journal of Applied Physics 109, 016110.

Zhao, K.J., Wang, W.L., Gregoire, J., Pharr, M., Suo, Z.G., Vlassak, J.J., Kaxiras, E., 2011c. Lithium-assisted plastic deformation of silicon electrodes in lithium-ion batteries: a first-principles theoretical study. Nano Letters 11, 2962–2967.